J. Fluid Mech. (1993), *vol.* 248, *pp.* 297–313

The rollup of a vortex layer near a wall

By JAVIER JIMÉNEZ[1,3] AND PAOLO ORLANDI[2,3]

[1] School of Aeronautics, U. Politécnica, Pl. Cardenal Cisneros 3, 28040 Madrid, Spain

[2] Dipartimento di Meccanica e Aeronautica, Università 'La Sapienza', Via Eudossiana 16, 00184, Roma, Italy

[3] Centre for Turbulence Research, Standford University, CA 94305, USA *and* NASA Ames Research Centre, CA 94035, USA

(Received 4 December 1991 and in revised form 8 September 1992)

The behaviour of an inviscid vortex layer of non-zero thickness near a wall is studied, both through direct numerical simulation of the two-dimensional vorticity equation at high Reynolds numbers, and using an approximate ordinary nonlinear integro-differential equation which is satisfied in the limit of a thin layer under long-wavelength perturbations. For appropriate initial conditions the layer rolls up and breaks into compact vortices which move along the wall at constant speed. Because of the effect of the wall, they correspond to equilibrium counter-rotating vortex dipoles. This breakup can be related to the disintegration of the initial conditions of the approximate nonlinear dispersive equation into solitary waves. The study is motivated by the formation of longitudinal vortices from vortex sheets in the wall region of a turbulent channel.

1. Introduction

The existence of streamwise vortical structures in the near-wall region of turbulent channels and boundary layers has been reported or inferred on many occasions during the last few decades. For example, the direct numerical simulations of channel flows by Kim, Moin & Moser (1987), using visualization techniques similar to those in the older experiments of Kim, Kline & Reynolds (1971), showed the existence of such structures with spacings and lengths similar to those observed in experiments. A more detailed study was done in Jiménez & Moin (1991) through the use of numerical simulations in 'minimal' channels, in which only a few structures are present in the computational domain, making it easier to follow their time evolution and interaction. These studies confirmed the essential character of the structures as long streamwise vortices, as well as their importance in determining the behaviour of the flow. A similar conclusion was reached by Robinson (1991) in his analysis of Spalart's (1988) turbulent-boundary-layer direct simulations. He observed that, in the inner zone, single unpaired near-wall quasi-streamwise vortices generate persistent low-speed streaks, and that counter-rotating vortex pairs are rare.

Thin localized layers of streamwise vorticity are also common features in the wall region, occurring most often near the outer edge of the viscous sublayer ($y^+ \approx 10$–15). They have thickness comparable with their distance from the wall, and spanwise widths of the same order as those of the low-velocity wall-layer streaks ($z^+ \approx 50$–100). As is true for most features near the wall, they are substantially longer than they are wide ($x^+ \approx 300$–500). They are observed to roll into compact streamwise cores that seem indistinguishable from the streamwise vortices mentioned above.

A particularly clear example is shown in figure 1, which is adapted from Sendstad

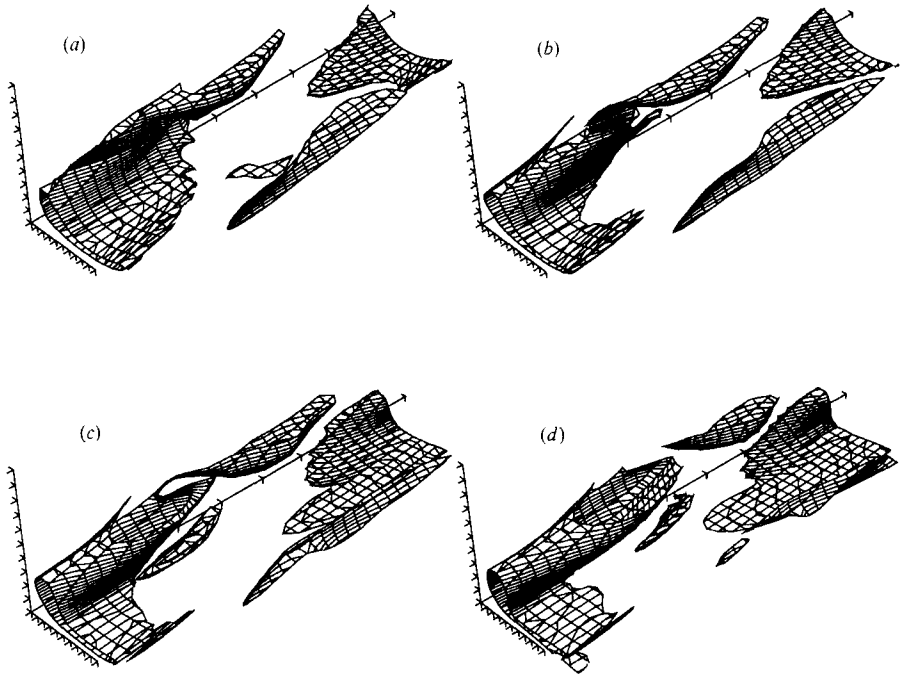

FIGURE 1. Rollup of a streamwise vortex layer, defined by an ω_x isosurface, in the wall region of a turbulent channel. Flow is from lower left to upper right. The domain is doubly periodic: $xu_\tau/\nu = 300$, $zu_\tau/\nu = 105$. $Re_\tau = 98$. The isosurface is $\omega_x \nu/u_\tau^2 = 0.1$; time between traces is $u_\tau^2 \Delta t/\nu = 9.5$, increasing from (*a*) to (*d*) (from Sendstad 1992).

(1992). It shows the time evolution of an isosurface of positive streamwise vorticity in the wall region of a minimal turbulent channel. The frame of reference moves forward with a translation velocity of 10 u_τ, close to the one associated with the high-stress features near the wall (Jiménez & Moin 1991). As a consequence the wall, which lies at the x, z coordinate plane, appears to move slowly backwards. The friction velocity is defined in terms of the average spanwise wall vorticity Ω, as $u_\tau = (\Omega\nu)^{\frac{1}{2}}$. The z, y coordinate plane at the lower left shows a cross-section of the structure. A vortex layer is observed, which rolls up later into a circular streamwise core with a thin tail to one side. More detailed cross-sections of these same fields, discussed in Sendstad (1992), show a strong streamwise vortex of opposite sign located on top of the vortex layer. Its rotation is such as to push the left edge of the layer towards the wall, so that the rollup of the far side of the layer occurs against the velocity induced by that vortex. This point will be discussed below in more detail. Sendstad also shows that, at the time of the last frame, secondary vorticity of opposite sign forms at the wall underneath the newly rolled vortex. Later, this secondary vorticity appears to organize itself into a new sheet, restarting the cycle. It is not clear whether the new sheet derives primarily from the secondary wall vorticity or from inviscid rotation of the other vorticity components in the flow. The analysis in Jiménez & Moin (1991) suggest that this latter alternative is the most likely one, and the issue is still under investigation. Here we will only concern ourselves with the rollup process, which occurs relatively far from the wall, and is almost certainly inviscid.

The fact that the dominant structures are elongated in the streamwise direction suggests that a quasi-two-dimensional model may be built, in the z, y transverse plane, in which the longitudinal variation is represented only by slow perturbation

terms. Two-dimensional flows can be studied at a level of detail that would be unaffordable in three dimensions and the mechanisms understood in this way can then be used as building blocks for the complete flow. A two-dimensional model for the rollup was introduced in Orlandi & Jiménez (1991), where the presence of the longitudinal vortices was also shown to be enough to account for many of the phenomena observed in near-wall turbulence, including the presence of low-velocity streaks and the growth of the mean wall shear stress above its laminar value. It was also observed in that paper that vortex layers introduced near the wall roll up into compact cores in times comparable with their eddy turnover times. The present paper is an attempt to explore this latter phenomenon and, although motivated by the wall turbulence observations, is mostly an investigation on a particular aspect of vorticity dynamics.

Pullin (1981) studied the behaviour of two-dimensional inviscid layers of uniform vorticity adjacent to a wall. His motivation was the formation of large-scale bulges at the outer edge of boundary layers. The scale of his flows was very different from ours, since they were intended to model the whole boundary layer, instead of the wall region, and his two dimensions were in the streamwise (x, y)-plane, as opposed to the transverse (z, y)-plane considered here but, from the point of view of vorticity dynamics, his computations are close to ours. His initial conditions were not appropriate to induce rollup. Stern & Pratt (1985) also investigated the evolution of an inviscid layer of uniform vorticity near a wall, with initial conditions close to ours and leading to rollup, but their interpretation and motivation were also somewhat different. We will discuss these results later.

A related 'collapse' of a vortex sheet into compact streamwise cores is known to occur away from walls, in the plane turbulent shear layer, and has been explained in Lin & Corcos (1984) and Neu (1984) as a result of the effect of longitudinal strain on the vortex layer. It had previously been shown by Lundgren (1982) that any axially strained flow in which the basic velocity field, except for the strain, is two-dimensional, can be related to a strictly two-dimensional flow field by a scaling transformation. This suggests that, even if the amplification of longitudinal vorticity in the shear layer is due to the presence of the straining field, the mechanism of rollup of the initial layer into compact cores is a two-dimensional one. In fact, two-dimensional numerical calculations of elongated vortices show a tendency to roll into cores (see Melander, McWilliams & Zabusky 1987, for a particular mechanism). A well known counterexample to this tendency, the equilibrium rotating elliptical Kirchhoff vortex of arbitrary elongation (Lamb 1932, §159), and its generalizations (Polvani & Flierl 1986), are probably isolated cases. From this point of view, the restriction imposed here that the layer be near a wall is a simplifying assumption, allowing for an approximate analytical treatment of the problem in the limit of thin layers with slow variations in the spanwise direction. However, the presence of the wall changes the character of the rollup, in that it becomes dominated by the influence of the 'image' vortex, reflected across the wall by the condition of zero normal velocity. Vortices near a wall behave like parts of counter-rotating dipoles rather than as independent entities.

The thin-layer analysis is presented in the next sections. The behaviour of the resulting equations is discussed, both analytically and numerically, and the important parameters identified. Simulations of the full two-dimensional equations of motion are also presented. They are not subject to the limitations of the approximate method, and provide a direct physical interpretation of the approximate results, as well as an evaluation of their accuracy. In particular, they show

that the local vorticity accumulations observed in the thin-layer approximation do indeed correspond to vortex rollup. It is shown that, for appropriate initial conditions, the vortex layer breaks into isolated equilibrium vortices which move along the wall at uniform velocity and without change of shape. This process is connected to the breakup of the solutions of the thin-layer equations into solitary waves, and this connection is explored. The relevance of this process to the behaviour of near-wall turbulence is discussed briefly in the conclusions.

2. The thin-layer approximation

Consider a two-dimensional flow near an infinite flat wall. In its application to wall turbulence, the two-dimensional plane would be the one normal to the mean flow, with only transverse variations being considered, while streamwise, x, derivatives are neglected. This will be emphasized by keeping throughout the paper the label z for the coordinate parallel to the wall. The flow is inviscid and incompressible and can be described by a velocity vector, (u, v), and a vorticity, $\omega = v_z - u_y$, which satisfy

$$\omega_t + u\omega_z + v\omega_y = 0, \tag{1}$$

where subscripts denote differentiation. The velocity satisfies the boundary conditions

$$v(z, y = 0) = 0, \quad u(z, y \to \infty) \to 0, \tag{2}$$

and can be computed from the vorticity using the Biot–Savart law,

$$u(z,y) = \frac{1}{2\pi}\int_{-\infty}^{\infty} \mathrm{d}\xi \int_0^{\infty} \omega(\xi,\eta)\left(\frac{(\eta-y)}{(\xi-z)^2+(\eta-y)^2}+\frac{(\eta+y)}{(\xi-z)^2+(\eta+y)^2}\right)\mathrm{d}\eta, \tag{3}$$

with an equivalent representation for v. The first term in the kernel of this integral represents the effect of the actual vorticity, while the second one corresponds to the negative image reflected by the wall to enforce the condition of zero normal velocity.

Note that the homogeneous boundary condition at infinity implies that there is no energy input to the flow and that the only equilibrium state is that at rest. Our interest will be in the evolution of an initial vorticity distribution. In a 'real' turbulent situation, three-dimensional effects have to be invoked to prevent the flow from decaying, and they would dominate the long-term behaviour. However, if the streamwise derivatives are much smaller than the transverse ones, the timescale associated with the three-dimensional effects, $\Delta x/U$, is much longer than the one associated to the transverse effects studied here, $\Delta z/U$, and the latter could still be observed as a fast transient phase within a slow three-dimensional evolution. It is in this light that the two-dimensional flows described here should be understood.

We will be interested in the case in which the vorticity is confined to a thin layer near the wall, for which $y \sim O(\epsilon) \ll 1$, but whose spanwise dimension is $\Delta z \sim O(1)$, and we will study the problem as a perturbation in the small parameter ϵ. To fix ideas, we choose the vorticity so that the spanwise velocity is $O(1)$. The relevant scalings are

$$z \sim u \sim O(1), \quad y \sim v \sim O(\epsilon), \quad \omega \sim O(1/\epsilon). \tag{4}$$

It is convenient to study the flow in terms of quantities integrated across the layer. Integrating (1) over $y \in (0, \infty)$, we obtain an evolution equation for the circulation density per unit span,

$$\frac{\partial \gamma}{\partial t} + \frac{\partial}{\partial z}\int_0^{\infty} u\omega \,\mathrm{d}y = 0, \tag{5}$$

where
$$\gamma(z) = \int_0^\infty \omega(z, y)\, \mathrm{d}y \sim O(1). \tag{6}$$

The velocity (3) can be put into a more convenient form by integrating by parts in z,

$$\left.\begin{aligned} u(z,y) &= u_0 + u_1, \\ u_0(z,y) &= \int_y^\infty \omega(z,\eta)\, \mathrm{d}\eta, \\ u_1(z,y) &= \frac{1}{2\pi}\int_{-\infty}^{\infty} \mathrm{d}\xi \int_0^\infty \frac{\partial \omega(\xi,\eta)}{\partial \xi}\left(\arctan\frac{\eta-y}{\xi-z} + \arctan\frac{\eta+y}{\xi-z}\right)\mathrm{d}\eta, \end{aligned}\right\} \tag{7}$$

where the branch of $\arctan(1/\xi)$ should be chosen so that it vanishes at $\xi \to \pm\infty$ and has a discontinuous jump at $\xi = 0$.

The main contribution to (7), within the vortex layer, is $u_0 \sim O(1)$. Using it in the convective vorticity flux in (5), we obtain a self-contained approximate evolution equation for γ, which behaves like a simple nonlinear wave,

$$\gamma_t + \gamma\gamma_z = 0. \tag{8}$$

This equation was first obtained by Stern & Paldor (1983) for the particular case of a layer of uniform vorticity, but the present derivation shows that it also applies to more general vorticity distributions (see also a recent discussion in Goldstein, Leib & Cowley, 1992). Its physical interpretation is that the vortex layer is too thin to perturb the outer flow, which remains at rest. The velocity, u_0, at the outer edge of the vortex layer is zero and increases by γ across the layer. The vorticity in the layer is convected by this spanwise velocity, averaged over its thickness, which is itself proportional to the circulation density. As a consequence, regions with higher circulation are convected faster, and they eventually overtake those with lower circulation, resulting in multiple-valued solutions for $\gamma(z)$ (Whitham 1974, pp. 19–26). Since γ is an integral over y and cannot be multivalued, a discontinuity has to appear, similar in some respects to the shocks in Burger's equation. It is important to note, however, that equation (8) is not Burgers' equation, and that the behaviour of the 'shock' is governed by higher-order terms that are not contained in this lowest-order approximation.

The exact correction to (8) is the small term, u_1, that was neglected in the expression for the velocity. That term is complicated but, in the interesting case of long waves ($\epsilon \ll 1$), it can be simplified by substituting the kernel,

$$K(\xi, y, \eta) = \arctan\frac{\eta-y}{\xi} + \arctan\frac{\eta+y}{\xi}, \tag{9}$$

by some approximation which is consistent with its limit as $\xi \gg \epsilon$,

$$K_\infty(\xi, y, \eta) = 2\eta \hat{K}_0(\xi), \tag{10}$$

with
$$\hat{K}_0(\xi) = 1/\xi. \tag{11}$$

The most serious discrepancy between (9) and (11) occurs near $\xi = 0$, where the latter becomes singular while the former is merely discontinuous. The behaviour of the kernel at small distances is related to the propagation of short waves. Equation (5) is inviscid, and any wave equation resulting from it is at most dispersive. A dispersion relation is defined when a uniform vortex layer is modified by infinitesimal perturbations proportional to $\exp[\mathrm{i}\kappa(x-ct)]$. It can be shown that the singularity of (11) at the origin leads to an infinite phase velocity for short waves and that that behaviour is spurious. Even if those waves cannot be expected to be described

correctly by a long-wave approximation, the infinite phase velocity interferes with the numerical analysis of the equation and introduces excessive dispersive effects in its evolution. The behaviour of short waves depends on the local dynamics of the vortex sheet, and on its internal structure.

To continue, we have to choose either a particular vorticity distribution across the layer, or an arbitrary form for our approximate kernel. Both approaches are consistent with the long-wave limit as long as the kernel tends to (10), (11) for large ξ.

The simplest application of the first approach is a layer with a uniform vorticity distribution, which leads to an integro-differential equation that is usually known as the contour dynamics equation (Deem & Zabusky 1978). That equation is exact, although complicated, but it can be integrated numerically. It has been applied to the case of a vortex layer adjacent to a wall by Pullin (1981), Stern & Pratt (1985) and Broadbent & Moore (1985) among others. It very quickly leads to overturning and filamentation, which are incompatible with the long-wave approximation, and which complicate the analysis of the solution. Both processes also result in engulfment of irrotational fluid, and eventually destroy the uniform distribution of vorticity. Our numerical experiments with full simulations of the Navier–Stokes equations support this behaviour for layers with moderate aspects ratios, $\epsilon \sim 1$, but suggest that entrainment is less important for thin slender layers, for which the constant-vorticity assumption should be more justifiable. In any case, it can only be considered as an arbitrary simplification intended to help to understand the basic structure of the rollup.

In this paper we have followed the second approach, which is to use a fully nonlinear approximation for the long-wave limit, and to choose the integral kernel so as to obtain a given linear dispersion relation for short waves. To simplify the comparison with previous work we have used the relation for a sheet of uniform vorticity, but the approach is more general and could be easily adapted to other cases.

The exact dispersion relation for infinitesimal waves on a uniform layer of constant vorticity, with thickness h and circulation density Γ, was obtained by Rayleigh (1887) as

$$c = \Gamma(1-\mathrm{e}^{-2\kappa h})/2\kappa h. \tag{12}$$

The phase velocity is always finite and approaches zero for very short waves, which is generally true for non-singular vorticity distributions. It can be reproduced exactly by the use of a kernel of the form (10), although with a different inner factor (see Appendix A),

$$\hat{K}_{\mathrm{e}}(\xi) = \frac{\pi}{2h} - \frac{\xi}{4h^2}\log\frac{\xi^2+4h^2}{\xi^2} - \frac{1}{h}\arctan\frac{\xi}{2h}. \tag{13}$$

In this kernel, $h \sim O(\epsilon)$ is the thickness of the layer, defined below in (15), and should strictly be taken as a variable quantity, depending on the local γ. There is no *a priori* reason to make h in $K(s-z)$ depend on $\gamma(s), \gamma(z)$, or on any other combination of the two, but it is analytically advantageous to choose a combination which is symmetric in (s,z), such as $0.5[\gamma(s)+\gamma(z)]$ (see Appendix B). This choice makes the equation highly nonlinear, but has the advantage of not introducing new parameters in the equation, and of leaving its scaling and symmetry properties intact. It should be remembered, in any case, that the resulting equation is only a simplified model for a complicated phenomenon, just as in the contour dynamics approximation, and that its only justification is to allow some analytical insights into the behaviour of the full equations.

Substituting (10) into the equation for u_1 leads to an evolution equation for the circulation, accurate to $O(\epsilon)$,

$$\frac{\partial\gamma}{\partial t}+\frac{\partial}{\partial z}\left(\frac{\gamma^2}{2}+\frac{\gamma}{\pi}\int_{-\infty}^{\infty}\frac{\partial\beta(s)}{\partial s}\hat{K}(s-z)\,\mathrm{d}s\right)=0, \tag{14}$$

where

$$\beta(z)=\int_0^{\infty} y\omega(z,y)\,\mathrm{d}y.$$

We consider now a vortex layer of constant vorticity $1/\pi\epsilon$ and local thickness $h(z)$,

$$\omega=1/\pi\epsilon \quad \text{if} \quad 0<y<h(z)=\pi\epsilon\gamma(z), \quad \omega=0 \text{ otherwise}, \tag{15}$$

and use it both to parameterize kernel (13) and to express β in terms of γ. The result is a model equation for the circulation which maintains the full nonlinear character of the problem and which has the right long- and short-wave dispersion properties,

$$\frac{\partial\gamma}{\partial t}+\frac{1}{2}\frac{\partial}{\partial z}\left(\gamma^2+\epsilon\gamma\int_{-\infty}^{\infty}\partial\gamma^2/\partial s\,\hat{K}_{\mathrm{e}}(s-z)\,\mathrm{d}s\right)=0, \tag{16}$$

It might be useful to comment again on the relation between the approximate equation (16) and the better known equations of contour dynamics, which are obtained in the present context by assuming uniform vorticity directly in (3). We have chose to introduce the assumption of uniform vorticity much later in the derivation to emphasize the relative generality of our approach. Equations (8) and (10) are strictly long-wave approximations that make no use of the vorticity distribution within the layer, as long as longitudinal gradients can be assumed to be small. Equation (14) is equally general, and it is only in closing it that a particular vorticity distribution has to be introduced. The assumption of uniform vorticity is the most convenient one, and probably the most physically relevant, but is not the only one possible. In fact any self-similar distribution of the form $\omega=F(y/h(z))$ results in an equation similar to (15) although with a different dispersive kernel. The price of this freedom is the need to abandon the accuracy for short waves, since different distributions have different high-wavenumber behaviour. It is because of this that we have to choose our kernel explicitly if we want to approximate a given vorticity distribution.

We might also comment at this point on the nonlinear character of the dispersive term in (16), since it might appear at first sight that it is a small term that can be linearized in γ without loss of accuracy. This is not so. The first nonlinear term in the equation, $\gamma\gamma_z$, is exact and implies no weakly nonlinear assumption, as follows from the derivation of (8). The only approximation is in the long-wave treatment of u_1, which depends only on the assumption that $\epsilon\sim\gamma^{-1}\gamma_z\ll 1$, but not on the smallness of the perturbations in γ. Other interesting limits are possible. Dritschel (1988), for example, uses a weakly nonlinear expansion of the contour dynamics equations of a circular vortex patch to study the behaviour of moderate-amplitude perturbations, and the resulting filamentation of the sharp interface. As discussed above, such short-wave phenomena are outside our approximation, but our results are not necessarily limited to weakly nonlinear perturbations, or to sharp interfaces. Stern & Pratt (1985) show that, for weakly nonlinear long waves, contour dynamics can be approximated by the Benjamin–Ono equation (Benjamin 1967), which is a version of (7) using the approximate kernel (11). As noted above, the dispersion relation for that kernel is incorrect for short waves.

3. Higher approximations and 'shock' structure

The lowest-order approximation discussed in the previous section is only valid as long as the horizontal derivatives remain small with respect to the normal ones. However, the presence of the nonlinear convection velocity in (8) guarantees that any initial distribution of γ will eventually generate locally high values of $\partial\gamma/\partial z$ at the points in which fluid particles with strong circulation overtake weak ones. At those points the low-order approximation breaks down and higher-order terms become important. The fact that (16) has no dissipative component suggests that it is unlikely to sustain steady-state 'shocks' similar to those in gas dynamics or in Burgers' equation. Dispersive equations tend to deal with discontinuities by emitting wave trains to get rid of the extra energy, in the same manner as in the undular bores of water waves (Whitham 1974, pp. 96–112).

In fact, it is possible to prove that (16) has no solutions corresponding to steady 'fronts' connecting two different uniform states with a wave of permanent form and constant celerity. The essence of the proof is that (16) can be shown to conserve the integral of an 'energy', γ^2, besides total circulation. When an equation can be written in conservation form,

$$\frac{\partial}{\partial t}\int_{-\infty}^{\infty}\rho\,\mathrm{d}z+\phi|_{-\infty}^{\infty}=0, \tag{17}$$

where the notation $\phi|_{-\infty}^{\infty}$ stands for $\phi(\infty)-\phi(-\infty)$, and ρ and ϕ represent some density and flux, it can be shown (Whitham 1974, pp. 30–32) that a smooth steady front connecting uniform states '+' and '−' should move with a velocity

$$u_{\mathrm{s}}=\frac{\phi_+-\phi_-}{\rho_+-\rho_-}. \tag{18}$$

Equation (16) is already in conservation form, for a density $\rho^{(1)}=\gamma$, and a flux $\phi^{(1)}=\frac{1}{2}\gamma^2$, since the integral term vanishes for a uniform state. This corresponds to vorticity conservation, and requires a front velocity

$$u_{\mathrm{s}}^{(1)}=\tfrac{1}{2}(\gamma_++\gamma_-), \tag{19}$$

It is shown in Appendix B that (16) can also be written as a conservation equation for $\rho^{(2)}=\gamma^2$, with a flux $\phi^{(2)}=\frac{2}{3}\gamma^3$. This conserved quantity, which is essentially β, can be related to the conservation of horizontal momentum. The corresponding front velocity,

$$u_{\mathrm{s}}^{(2)}=\tfrac{2}{3}(\gamma_+^3-\gamma_-^3)/(\gamma_+^2-\gamma_-^2), \tag{20}$$

is in general different from that given in (19) and, since a permanent front can only have one propagation velocity, either one or the other quantity would not be conserved by it, and permanent fronts are impossible.

Note that, to be able to derive a front velocity, conservation has only to be proved in infinite domains, as in (17). Strict conservation requires that the same result applies between arbitrary limits. As noted by one of the referees, the first conservation law discussed above is strict, while the second one applies only in the weak sense discussed in this paragraph.

Physically, the root of the problem is the difference between the velocity with which a discontinuity is being convected by the flow and the vorticity conservation velocity (19). Consider a weak front connecting two uniform vortex layers with circulation densities γ_+ and γ_-. If the vorticity in both layers is the same, the

different circulations are the result of different thickness, and the front appears as a jump in the upper surface of the layer. A sharp front is convected with the local velocity of the fluid, since it can be essentially identified with a fluid particle, and that velocity is small near the upper interface. It is only the collective effects associated with large wavelengths that can induce phase velocities appreciably different from those of the local fluid. That is why the exact dispersion relation (12) vanishes as $\kappa \to \infty$. In fact, the velocity induced by a rectangular step on the surface of a vortex layer can be computed exactly by conformal mapping, with the result that the fluid at the centre of the step moves approximately with a velocity $\frac{1}{2}|\gamma_+ - \gamma_-|$. This is roughly the convection velocity of a weak shock, and is small and in general different from (19). As a consequence vorticity is not conserved and it is this lack of conservation that leads to a local accumulation of vorticity near the front, and to the rollup. The length over which the rollup is spread is controlled by the difference between the slow convection velocity of the shock and that of the bulk of the vorticity, which is proportional to the local circulation density. For weak fronts in strong layers this difference is large, and the fronts disperse fast, without leading to strong rollups. Conversely, strong shocks on weak layers remain compact, leading to strong vorticity concentrations. Examples of this, and other, behaviour are shown in the numerical simulations in the next section.

These remarks help to explain the sequence of events in figure 1. Consider the vortex layer lying near the wall in frame (*a*). Its vorticity is clockwise ($\omega < 0$), and it induces near the wall velocities directed towards the left (far) side of the channel. This is also the edge at which the layer eventually rolls up. The velocity field adjusts itself to a state of rest (or uniform velocity) away from the wall, and does so by creating a variable left-going jet between the vortex layer and the wall, which is the one that eventually produces the rollup. Note that this is true even in the presence of a no-slip wall that reacts to the jet by creating a secondary vortex sheet of opposite sign, which is not shown in our three-dimensional figure but which is clearly visible in the two-dimensional sections given in Sendstad (1991). It should also be emphasized that, as noted in the introduction, the rollup develops in a direction opposite to that induced by other vortices in the flow field, and that it should therefore be considered as a consequence of the nonlinear interaction of the layer with itself.

4. Simulation results

In this section we present results from two sets of numerical simulations. Those in the first group solve the initial value problem for the approximate nonlinear integro-differential equation (16), with the kernel (13). They use a simple finite-differences, second-order scheme, either with periodic boundary conditions in z or with the assumption that γ is constant outside the domain of integration. The result is a time history for the circulation density, $\gamma(z, t)$. Because of the assumptions that went into the derivation of (16), these simulations approximate a uniform vorticity distribution across the layer.

The second set of simulations integrate the initial value problem for the full two-dimensional Navier–Stokes equations (1)–(3), with a Reynolds number and free-slip conditions at the wall, $\omega(z, y = 0) = 0$. As a consequence, the flow is essentially inviscid and should be qualitatively comparable to that in the first set of simulations. The numerical scheme is described in detail in Orlandi (1989). It is a finite-differences, vorticity–streamfunction code, with second-order accuracy in both space

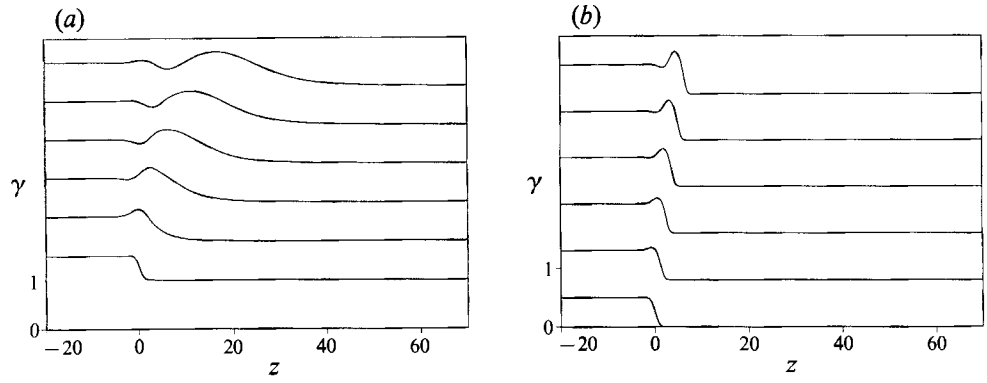

FIGURE 2. Evolution of a front in the circulation density, γ, according to (16). $\epsilon = 0.5$; time between traces, $\Delta t = 6$, running upwards. (*a*) $\gamma_- = 1.5$, $\gamma_+ = 1$; (*b*) $\gamma_- = 0.5$, $\gamma_+ = 0$.

and time. It uses explicit time advancing for the nonlinear terms, but is fully implicit for the viscous ones, with global conservation of enstrophy, energy and circulation in the inviscid limit. We use grids of up to 257×1537 ($z \times y$), to represent accurately the high vorticity gradients that are needed to approximate a uniform vorticity distribution. Some smoothing at the vortex boundaries is nevertheless necessary, and is carried out using a hyperbolic tangent function with a thickness of about 10% of the layer thickness. The condition at $y \to \infty$ is simulated by a free-slip horizontal boundary in the irrotational region away from the wall. The horizontal size of the numerical domain, and the vorticity magnitude are chosen so as to be comparable with the simulations in the first set. The resulting vortex-layer thickness and maximum vorticity are both $O(1)$. The location of the upper numerical boundary was found to influence appreciably the convection velocity of the structures, and was increased until the error in the velocity was below 1%. The resulting numerical domain is $z = 50$, $y = 20$. The Reynolds number, defined as the ratio of total circulation in the computational box to the kinematic viscosity, is 10^4. The flow is assumed to be periodic in the z-direction.

The results of this second set of simulations are two-dimensional vorticity maps. From them, the circulation density, γ, can be computed by integration over y and compared with the results of (16). The main purpose of these simulations, however, is not to check the accuracy of that equation, but to gain insight into the vorticity distributions leading to the different effects observed in the evolution of γ. This is done by comparing the one-dimensional circulation distribution with the two-dimensional vorticity maps.

An example of the two different types of front behaviour discussed at the end of the previous section is shown in figure 2, which was obtained by numerical integration of (16). A strong front representing the leading edge of a uniform vortex layer quickly develops a concentrated vortex at its leading edge, while another one, representing a change of intensity within a relatively strong layer disperses into longer waves which can hardly be described as concentrated. Similar behaviour was found by Stern & Pratt (1985) using contour dynamics for a uniform sheet. They, however, interpret them as steady shocks and try to explain the velocity of the concentrated vortices in terms of a shock-fitting formula of the type discussed in §3. For the reasons explained in that section we believe that to be incorrect, and we will give below an interpretation of the vortices in terms of nonlinear solitary waves of the dispersive equation.

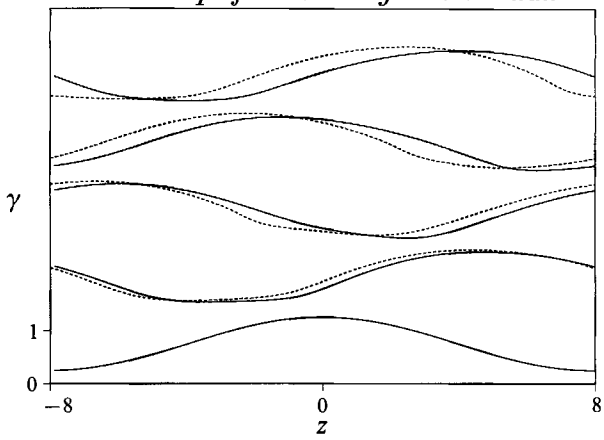

FIGURE 3. Evolution of the circulation density, γ, in a spatially periodic vortex sheet. Solid lines, approximate equation (16); dashed, direct simulation of (1). $\epsilon = 0.5$; $\gamma(z,0) = 0.75+0.5\cos(\pi z/8)$; time interval between traces, $\Delta t = 10$, running upwards.

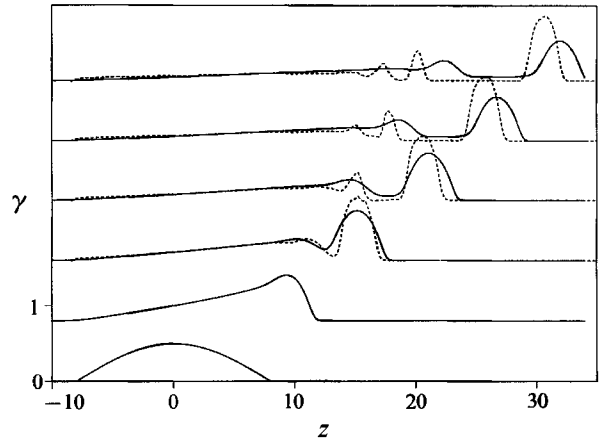

FIGURE 4. Evolution of the circulation density, γ, in an isolated vortex layer. $\epsilon = 0.5$; $\gamma(z,0) = 0.5\cos(3\pi z/50.)$ if $|z| < 25/3$), zero otherwise; time interval between traces, $\Delta t = 30$, running upwards. Solid lines, equation (16); dashed, direct simulation.

Two other examples are given in figures 3–5. In figure 3, a layer with a sinusoidal perturbation disperses without rolling up. Circulation distribution histories both from the approximate equation and from direct simulations are shown, and they agree qualitatively. The vorticity fields of the direct simulation are uninteresting, and show a slightly nonlinear wave propagating from left to right. There is no significant entrainment of irrotational fluid. This was the case treated by Pullin (1981), using contour dynamics, although for shorter wavelengths. He did not find rollup, but his waves steepened and developed thin irrotational filaments that were entrained into the layer. Our numerical simulations of shorter waves show the same results, but they are outside the scope of this paper, and they are not shown here. The reason for the absence of rollup is the same as in the case of the circulation front within a strong layer. Any sharp longitudinal derivative formed by the flow travels with a celerity close to the (zero) velocity of the free stream, and is immediately dispersed by the long nonlinear waves travelling at much higher phase speeds.

A more interesting example is that in figure 4 which displays the evolution of an isolated vortex layer, and is closer to the turbulent channel features that motivated

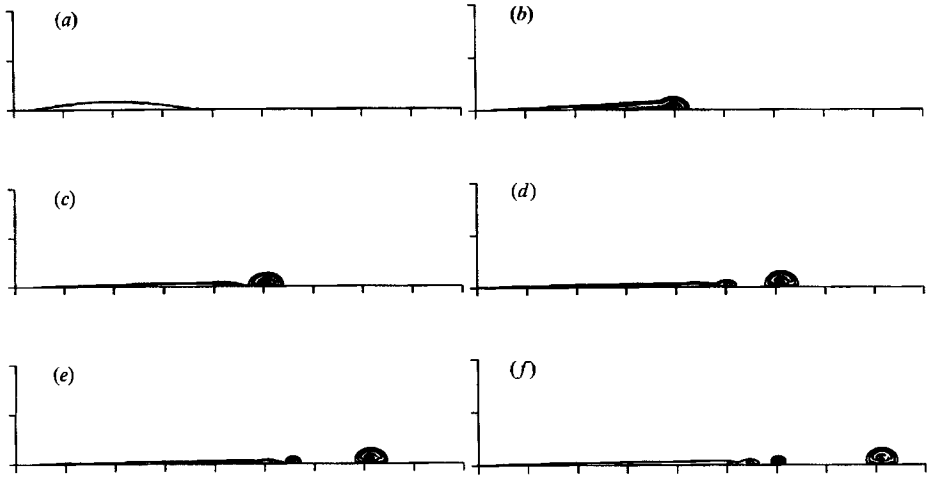

FIGURE 5. Vorticity maps corresponding to the direct simulations in figure 4. Horizontal axis at wall, $z \in (-10, 35)$. Time increases from (a)–(f).

our research. A strong discontinuity at its leading edge appears which eventually results in an accumulation containing most of the vorticity in the layer. A secondary rollup is observed behind the primary one, and eventually the layer breaks into a leading vortex, with a completely disconnected, smaller, secondary one behind it. Note that the left-hand end of the layer does not move during the evolution, in agreement with the zero propagation velocity implied by (8) for points at which $\gamma = 0$. As a consequence, the rolled vortices retain a thin 'tail' formed by the slowly moving vorticity from the left end of the original layer.

These effects are even more pronounced in the results of the direct two-dimensional simulations, which are shown as dashed lines in figure 4 and as two-dimensional maps in figure 5. The breaking of the layer into isolated vortices is here more complete and, in the last time frame, three individual vortices can be identified. The trailing tail is also present and stagnant. The qualitative behaviour of the two solutions in figure 4 is similar, but their quantitative agreement is poor. This had to be expected, not only because the vorticity distribution of the direct simulations is not exactly uniform, but also because the geometrical aspect ratio of the leading vortex in figure 5 is $h/L \approx 0.4$, well beyond the limit of validity of the long-wave approximation that led to (16).

5. Solitary waves and vortex dipoles

The process by which the layer in figures 4–5 breaks into isolated vortices, both in the solutions of the approximate equation (16) and in the direct simulations, is interesting and had not, to our knowledge, been reported previously, although its initial stages had been described for fronts in Stern & Pratt (1985). It brings to mind the breakup of the initial conditions of some nonlinear dispersive systems into solitary waves and, indeed, the structures appear to preserve their shape for long times once they are separated from the initial layer.

These structures can be identified immediately as shape-preserving vortices which, because of the presence of the wall, form part of counter-rotating, touching dipoles. This is confirmed by the vorticity maps in figure 5, where they appear as almost semi-

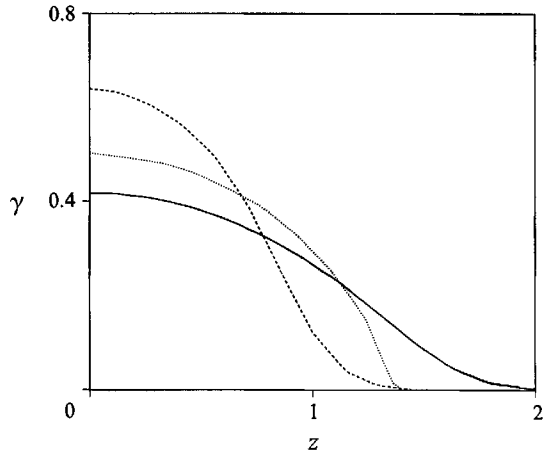

FIGURE 6. Circulation density for solitary waves (vortex dipoles), normalized to unit total circulation and $\omega = 2/\pi$. Solid line, equation (16); dashed, equation (1); dotted, Pierrehumbert (1980).

elliptical vortices travelling along the wall. Steady propagating solutions for touching dipoles with uniform vorticity were computed in Sadovskii (1971) and Pierrehumbert (1980). They form a geometrically similar family, parameterized by the vorticity ω and the area S, and they move with a translation velocity $c = 0.164\,\omega S^{\frac{1}{2}}$ (Saffman & Tanveer 1982). Saffman & Szeto (1980) quote experimental evidence showing that these dipoles, when produced as perfectly symmetrical structures by the presence of a wall, are very stable, in agreement with the results of our calculations.

The solitary waves of (16), if they are really permanent, should also form a geometrically similar family. There is only one lengthscale in the flow, and the Saffman–Tanveer formula for the propagation velocity should be satisfied, $c = k_2(\Gamma/\pi\epsilon)^{\frac{1}{2}}$, where Γ is the total circulation contained in the structure. It follows from the numerical experiments that $k_2 \approx 0.158$, which is in fair agreement with the exact value given above.

The solitary structures produced by the exact two-dimensional equations and by (16) are compared in figure 6, together with the circulation distribution for the Pierrehumbert dipole. The agreement is only qualitative. An examination of the detailed vorticity distributions shows that the direct numerical simulations differ from the uniform dipole mainly because of the smoothing of the vorticity near the edges, while it has already been noted that the solitary waves are outside the range of quantitative agreement of the long-wave approximation of (16).

It should be noted, finally, that the numerical experiments reported here do not constitute a proof for the existence of solitary permanent solutions to (16). A rigorous proof requires the computation of permanent waves as such, not as limits of the initial-value problem. The evolution experiments, however, serve as useful indications of which types of permanent solutions are likely to exist, and these can in turn be used as a guide in the search for solutions of the two-dimensional equations. It is therefore interesting to inquire whether other permanent solutions exist besides the solitary waves and the corresponding vortex dipole. Two obvious candidates are periodic nonlinear wave trains and solitary waves whose circulation does not decay to zero as $|z|$ goes to infinity. The former would correspond to trains

of linked dipoles, while the latter would represent a compact vortex riding on a uniform layer, or pedestal. Preliminary numerical experiments, such as those contained in figure 3, suggest that the former exist, and indeed Broadbent & Moore (1985) describe a family of permanent periodic waves to the contour dynamic equations. Numerical evolution experiments, with initial conditions which could be expected to generate solitary pedestal solutions of (16), appear to generate almost self-similar solitary waves which spread slowly until they merge into the background circulation. On the other hand, Stern & Pratt show that a weakly linear version of (16), using kernel (11), can be related to the Benjamin–Ono equation (Benjamin 1967) which is known to have soliton solutions. Following these leads, recent calculations of permanent solutions to the contour dynamics equations have identified a family of solitary waves with non-zero pedestal, which tend almost everywhere to the Pierrehumbert dipole in the zero pedestal limit (Higuera & Jiménez, 1992).

6. Conclusions

We have shown that a vortex layer of finite longitudinal extent in the neighbourhood of a slip wall tends to roll into discrete vortices which move along the wall without change in shape or in translation velocity. It had been reported previously by Pullin (1981) that infinite periodic connected sheets do not roll up, and our computations confirm that conclusion. We have also shown that the qualitative behaviour of the layer can be described by means of a nonlinear dispersive ordinary integro-differential equation that is satisfied by the layer in the long-wave limit. The accumulation of vorticity that leads to rollup can be linked to the appearance of discontinuous solutions of the lowest-order approximation, which satisfies the equation for nonlinear kinematic waves. The subsequent behaviour is explained by the properties of the dominant dispersive term of the next-order approximation and, in particular, by the existence of extra conservation laws for the new approximate equation that prohibit the existence of steady fronts.

The disintegration of the layer into individual vortices corresponds to the breaking of the solutions of the approximate equation into solitary waves. The vortices themselves, being close to a slip wall, behave like the counter-rotating dipoles computed by Sadovskii (1971) and Pierrehumbert (1980).

The motivation of our investigation was the observation by Sendstad (1992) that vortex layers in the wall region of turbulence flows appear to roll into streamwise vortices, which have been shown repeatedly to be the dominant structures in this flow region and, in particular, to be responsible for much of the extra drag of turbulent flows (Orlandi & Jiménez 1991). The results in this paper show that the rollup is a plausible mechanism, and that it can be explained in purely two-dimensional terms in the cross-stream plane, although three-dimensional effects would eventually have to come into play to prevent the vortices from decaying through viscous diffusion. The rollup mechanism is inviscid and linked to the presence of the wall through the effect of the reflected vorticity. It evolves on a timescale comparable to the inertial time of the vortex layer. This suggests that any effort to control wall turbulence by preventing the formation of the longitudinal vortices should concentrate either on preventing the formation of the vortex layers near the wall, or on dissipating them once they form. We suggest that this may be one of the mechanisms by which riblets decrease the friction coefficient of turbulent boundary layers. The fact that, when undisturbed, the layers seem to lie at the edge

of the viscous region, $y^+ = 10$–15, may help to explain why riblets of about that height are particularly effective.

Much of this work was carried out while the authors were working at the Centre for Turbulence Research, whose support is gratefully acknowledged. We are especially indebted to the fruitful discussions with O. Sendstad on the motivation of this research, and for his permission to use figure 1. We have also benefited from discussions with G. B. Whitham and F. Higuera on the solutions of equation (16). P. O. was supported in part with funds by the M. P. Italiano, and J. J. by the Hermes program of the ESA, under contract AMD-RDANE 3/88, and by a grant from United Technologies Corporation. We are indebted to K. Shariff for many useful suggestions on a draft version of this manuscript.

Appendix A. Linear dispersion relations

Linearizing (16) around $\gamma(z) = \Gamma + \gamma'(z)$, where the second term is assumed to be much smaller than the first, we obtain

$$\frac{\partial \gamma'}{\partial t} + \Gamma \frac{\partial}{\partial z}\left(\gamma' + \epsilon\Gamma \int_{-\infty}^{\infty} \frac{\partial \gamma'}{\partial s} \hat{K}(s-z)\,\mathrm{d}s\right) = 0, \tag{A 1}$$

where γ' has to be substituted by $\exp[\mathrm{i}\kappa(z-ct)]$. The dispersion relation between c and κ can be written as

$$\frac{c}{\Gamma} = 1 - \frac{2\kappa h}{\pi} \int_0^{\infty} \sin(\kappa h \xi)\, Q(\xi)\,\mathrm{d}\xi, \tag{A 2}$$

where $h = \pi\epsilon\Gamma$ is the thickness of the unperturbed layer, and $Q(\xi) = h\hat{K}(h\xi)$ is a normalized form of the kernel. For the kernel defined in (11),

$$\hat{K}_0(\xi) = Q_0(\xi) = 1/\xi, \quad c_0 = \Gamma(1-\kappa h), \tag{A 3}$$

whereas the exact dispersion relation for a layer of uniform vorticity nearby is given by (12)

$$c_{\mathrm{e}} = \Gamma(1-\mathrm{e}^{-2\kappa h})/2\kappa h. \tag{A 4}$$

In the long-wave limit, $\kappa h \ll 1$, the two dispersion relations behave similarly, differing only at $O(\kappa^2)$. In the high-wavenumber limit, the exact relation decays to zero like

$$c_{\mathrm{e}} \approx \Gamma/2\kappa h, \tag{A 5}$$

while (A 3) decreases linearly to $-\infty$.

In fact, the sine transform in (A 2) can be inverted to obtain a kernel with a given dispersion relation,

$$Q(\xi) = \int_0^{\infty} \frac{1 - c(\kappa)/\Gamma}{\kappa} \sin(\kappa h \xi)\,\mathrm{d}\kappa. \tag{A 6}$$

The kernel corresponding to (A 4) is, for $\kappa \geqslant 0$,

$$Q_{\mathrm{e}}(\xi) = \tfrac{1}{2}\pi - \tfrac{1}{4}\xi \log[(\xi^2+4)/\xi^2] - \arctan(\tfrac{1}{2}\xi), \tag{A 7}$$

where the branch of the arctangent should be chosen so that it vanishes at the origin. Far from the origin, $\hat{K}_{\mathrm{e}} \to 1/\xi$, while in the limit of $\xi = 0$ it has a simple discontinuity, $\hat{K}_{\mathrm{e}}(0\pm) = \pm\pi/2h$.

Appendix B. Conservation laws

Equation (15) is already in conservation form. Consider a solution such that $\gamma(z) \to \gamma^{\pm}$ as $z \to \pm\infty$, and integrate (15) over $z \in (-\infty, \infty)$. Note that the last term in the equation vanishes at infinity because the derivative in the integrand vanishes. The first conservation law, which corresponds to vorticity conservation, is

$$\frac{\partial}{\partial t}\int_{-\infty}^{\infty} \gamma(z)\,\mathrm{d}z + \frac{\gamma^2}{2}\Big|_{-\infty}^{\infty} = 0.$$

To obtain the second conservation law, multiply (15) by 2γ, and integrate over $z \in (0, \infty)$. The first two terms in the equation are easily converted into conservation form, while the integral term becomes

$$\int_{-\infty}^{\infty} 2\gamma(z)\,\mathrm{d}z \frac{\partial}{\partial z}\left(\gamma(z)\int_{-\infty}^{\infty} \frac{\partial \gamma^2}{\partial s}\hat{K}(s-z)\,\mathrm{d}s\right),$$

which can be integrated by parts – in z – to obtain

$$\int\int_{-\infty}^{\infty} \frac{\partial \gamma^2}{\partial z}\frac{\partial \gamma^2}{\partial s}\hat{K}(s-z)\,\mathrm{d}s\,\mathrm{d}z.$$

This integral has the form

$$\int\int_{-\infty}^{\infty} F(z)\,F(s)\,\hat{K}(s-z)\,\mathrm{d}s\,\mathrm{d}z,$$

and vanishes because of antisymmetry in (z, s). The resulting conservation equation can be written as

$$\frac{\partial}{\partial t}\int_{-\infty}^{\infty} \gamma^2\,\mathrm{d}z + \frac{2\gamma^3}{3}\Big|_{-\infty}^{\infty} = 0.$$

Note that this derivation is only valid for those cases in which $\hat{K}$ is independent of γ, or in which the dependence is such that $\hat{K}(s-z)$ remains antisymmetric in (s, z).

REFERENCES

Benjamin, T. B. 1967 Internal waves of permanent form in fluids of great depth. *J. Fluid Mech.* **29**, 559–592.

Broadbent, E. G. & Moore, D. W. 1985 Waves of extreme form on a layer of uniform vorticity. *Phys. Fluids* **28**, 1561–1563.

Deem, G. S. & Zabusky, N. J. 1978 Vortex waves: stationary V-states, interactions, recurrence and breaking. *Phys. Rev. Lett* **40** 859–862.

Dritschel, D. G. 1988 The repeated filamentation of two-dimensional vorticity interface. *J. Fluid Mech.* **194**, 511–547.

Goldstein, M. E., Leib, S. J. & Cowley, S. J. 1992 Distortion of a flat plate boundary layer by a free stream vorticity normal to the plate. *J. Fluid Mech.* **237**, 231–260.

Higuera, F. & Jiménez, J. 1992 Solitary waves on planar and axisymmetric vorticity layers. *J. Fluid Mech.* (submitted).

Jiménez, J. & Moin, P. 1991 The minimal flow unit in near wall turbulence. *J. Fluid Mech.* **225**, 213–240.

Kim, H. T., Kline, S. J. & Reynolds, W. C. 1971 The production of turbulence near a smooth wall in a turbulent boundary layers. *J. Fluid Mech.* **50**, 133–160.

Kim, J., Moin, P. & Moser, R. 1987 Turbulence statistics in fully developed channel flow at low Reynolds number. *J. Fluid Mech.* **177**, 133–166.

LAMB, H. 1932 *Hydrodynamics*. Cambridge University Press.

LIN, S. J. & CORCOS, G. M. 1984 The mixing layer: deterministic models of a turbulent flow. Part 3. The effect of plane strain on the dynamics of streamwise vortices. *J. Fluid Mech.* **141**, 139–178.

LUNDGREN, T. S. 1982 Strained spiral vortex model for turbulent fine structure. *Phys. Fluids* **25**, 2193–2203.

MELANDER, M. V., MCWILLIAMS, J. C. & ZABUSKY, N. J. 1987 Axisymmetrisation and vorticity gradient intensification of isolated two dimensional vortices through filamentation. *J. Fluid Mech.* **178**, 137–159.

NEU, J. 1984 The dynamics of stretched vortices. *J. Fluid Mech.* **143**, 253–276.

ORLANDI, P. 1989 Numerical simulation of vortices motion in presence of solid boundaries. In *Proc 8th GAMM Conf. on Numerical Methods in Fluid Mechanics* (ed. P. Weeseling) pp. 436–441. Vieweg, Braunschweig.

ORLANDI, P. & JIMÉNEZ, J. 1991 A model for bursting of near wall vortical structures in boundary layers. In *8th Symp. Turbulent Shear Flows, Munich, Sept. 9–11, 1991*, pp. 28.1.1–28.1.6.

PIERREHUMBERT, R. T. 1980 A family of steady, translating vortex pairs with distributed vorticity. *J. Fluid Mech.* **99**, 129–144 (and Corrigendum. *J. Fluid Mech.* **102**, 478).

POLVANI, L. M. & FLIERL, G. R. 1986 Generalised Kirchhoff vortices. *Phys. Fluids* **29**, 2376–2379.

PULLIN, D. I. 1981 The nonlinear behaviour of a constant vorticity layer at a wall. *J. Fluid Mech.* **108**, 401–421.

RAYLEIGH, LORD 1887 On the stability or instability of certain fluid motions, II. *Scientific Papers*, vol 3, pp. 17–23. Cambridge University Press. Also *Proc. Lond. Math. Soc.* **19**, 67–74.

ROBINSON, S. K. 1991 Coherent motions in the turbulent boundary layer. *Ann. Rev. Fluid Mech.* **23**, 601–639.

SADOVSKII, K. S. 1971 Vortex regions in a potential stream with a jump of Bernouilli's constant at the boundary. *Prik. Matem. Mekh.* **35**, 773–779.

SAFFMAN, P. G. & SZETO, R. 1980 Equilibrium shapes of a pair of equal uniform vortices. *Phys. Fluids* **23**, 2339–2342.

SAFFMAN, P. G. & TANVEER, S. 1982 The touching pair of equal and opposite uniform vortices. *Phys. Fluids* **25**, 1929–1930.

SENDSTAD, O. 1992 Mechanics of three dimensional boundary layers. PhD thesis, Stanford University.

SPALART, P. R. 1988 Direct numerical simulation of a turbulent boundary layer up to $R_\theta = 1410$. *J. Fluid Mech.* **187**, 61–98.

STERN, M. E. & PALDOR, N. 1983 Large amplitude long waves in shear flow. *Phys. Fluids* **26**, 906–919.

STERN, M. E. & PRATT, L. J. 1985 Dynamics of vorticity fronts. *J. Fluid Mech.* **161**, 513–532.

WHITHAM, G. B. 1974 *Linear and Nonlinear Waves*. John Wiley.